

Article

One Pot Synthesis of Copper Oxide Nanoparticles for Efficient Antibacterial Activity

Rajaram Rajamohan ^{*}, Chaitany Jayprakash Raorane, Seong-Cheol Kim ^{*} and Yong Rok Lee ^{*}

School of Chemical Engineering, Yeungnam University, Gyeongsan 38541, Republic of Korea

^{*} Correspondence: rajmohanau@yu.ac.kr (R.R.); sckim07@ynu.ac.kr (S.-C.K.); yrlee@yu.ac.kr (Y.R.L.)

Abstract: The unique semiconductor and optical properties of copper oxides have attracted researchers for decades. However, using fruit waste materials such as peels to synthesize the nanoparticles of copper oxide (CuO NPs) has been rarely described in literature reviews. The main purpose of this part of the research was to report on the CuO NPs with the help of apple peel extract under microwave irradiation. Metal salts and extracts were irradiated at 540 W for 5 min in a microwave in a 1:2 ratio. The crystallinity of the NPs was confirmed by the XRD patterns and the crystallite size of the NPs was found to be 41.6 nm. Elemental mapping of NPs showed homogeneous distributions of Cu and O. The NPs were found to contain Cu and O by EDX and XPS analysis. In a test involving two human pathogenic microbes, NPs showed antibacterial activity and the results revealed that the zone of inhibition grew significantly with respect to the concentration of CuO NPs. In a biofilm, more specifically, NPs at 25.0 µg/mL reduced mean thickness and biomass values of *S. aureus* and *E. coli* biofilms by >85.0 and 65.0%, respectively, with respect to untreated controls. In addition, environmentally benign materials offer a number of benefits for pharmaceuticals and other biomedical applications as they are eco-friendly and compatible.

Keywords: microwave-assisted synthesis; CuO; XPS analysis; BET; antimicrobial activity; biofilm



Citation: Rajamohan, R.; Raorane, C.J.; Kim, S.-C.; Lee, Y.R. One Pot Synthesis of Copper Oxide Nanoparticles for Efficient Antibacterial Activity. *Materials* **2023**, *16*, 217. <https://doi.org/10.3390/ma16010217>

Academic Editors: Alexandru Mihai Grumezescu and Paul Cătălin Balaure

Received: 25 November 2022
Revised: 14 December 2022
Accepted: 21 December 2022
Published: 26 December 2022



Copyright: © 2022 by the authors. Licensee MDPI, Basel, Switzerland. This article is an open access article distributed under the terms and conditions of the Creative Commons Attribution (CC BY) license (<https://creativecommons.org/licenses/by/4.0/>).

1. Introduction

Infections caused by bacteria are a growing public health concern and are the major reason for the spread of serious diseases worldwide, with millions of new cases and deaths per year [1,2]. Fresh products contaminated with bacteria are the most common source of bacterial illnesses. Therefore, individual consumers, industries, and regulatory authorities are concerned about food safety. Most commonly, *Salmonella*, *Escherichia coli*, and *Staphylococcus aureus* cause foodborne illnesses [2,3]. It is possible for people to experience diarrhea, abdominal cramps, and nausea after consuming food that contains these pathogenic bacteria. As a result, it may also cause chronic illnesses such as cancer, brain disorders, kidney failure, and liver failure [4]. Bacterial infections caused by these microorganisms remain a challenge because they often form biofilms on surfaces and have developed an enhanced resistance to commonly used antimicrobial agents [5]. Drying, pickling, thermal processing, and freezing are traditional methods of extending food shelf life. As a result of these procedures, most nutrients in food are denaturalized or destroyed [6].

Metal oxides are widely used in modern technology owing to their excellent electrical, chemical, and optical properties [7,8]. Furthermore, metal oxide nanoparticles are increasingly being investigated for their biological properties. Several researchers have assessed the biologically effective activity of nanoparticles of metal oxide, especially copper oxide (CuO), which have established improved biological activity in comparison with metal NPs [9]. Among the various metal and their oxide-based NPs, copper has gained recognition due to its high redox potential [10]. Copper-based NPs such as CuO, amorphous and crystalline CuS, CuPO₄, and CuI is reported to have biological activity [11–15].

A variety of physical and chemical routes have been used to obtain CuO NPs with desired morphologies [16–20]. It is important to note, however, that these methods require a lot of labor, a lot of energy, an intensive route, and hazardous chemicals [21]. It is, therefore, essential that new biocompatible approaches be developed that can help to rectify the above-mentioned limitations [22]. The synthesis of NPs including metal as well as metal oxide is shifting from physical and chemical methods to biological methods termed biosynthesis or green synthesis [23,24]. Recently, fruit peels have been used to synthesize metal or metal oxide nanoparticles [25–27]. Due to its sustainability, cost-effectiveness, and simplicity, the photosynthesis of CuO NPs has gained more attention recently [28]. The purpose of this research work was to provide an environmentally friendly synthetic process for CuO NPs characterization followed by an antibacterial activity.

To the best of our knowledge, there are no other reports on the synthesis of CuO NPs with the help of apple peel extracts via microwave irradiation. The obtained NPs were characterized by analytical techniques which include XRD, FE-SEM, HR-TEM, XPS, and BET surface analysis. Moreover, our aim from the application point of view was to test the antimicrobial and antibiofilm efficacy of synthesized CuO NPs against Gram-positive as well as Gram-negative bacterial pathogens.

2. Materials and Methods

2.1. Materials

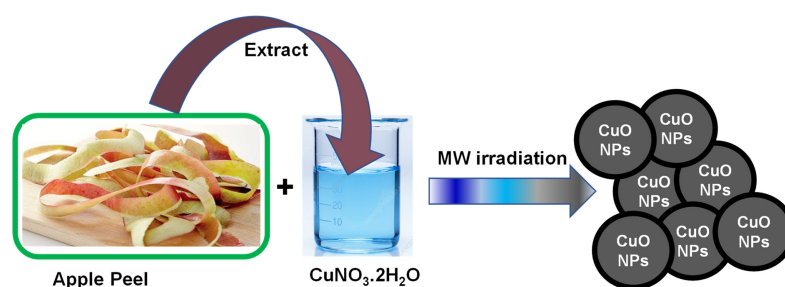
The Sigma Aldrich Company, Seoul, Republic of Korea, provided copper nitrate (molecular formula: $\text{CuNO}_3 \cdot 2\text{H}_2\text{O}$, Purity: >99%) for the synthesis of NPs without further purification. The $\text{CuNO}_3 \cdot 2\text{H}_2\text{O}$ was readily soluble in distilled water. After thoroughly washing the glassware with distilled water, they were dried in the oven for 30.0 min to avoid contamination of the glassware by the deposition of impurities.

2.2. Preparation of Apple Peel Extract

From the fresh and delicious apples, apple peel extract has been prepared with the help of a homogenizer. A detailed procedure has been given in the Supplementary Materials.

2.3. Preparation of CuO NPs

AP extract (10.0 mL) and $\text{CuNO}_3 \cdot 2\text{H}_2\text{O}$ (3.146 g in 50.0 mL distilled water) were taken separately with the required amounts. A scheme for synthesizing NPs is shown in Scheme 1. An extract of AP was typically added directly to aqueous solutions of $\text{CuNO}_3 \cdot 2\text{H}_2\text{O}$ at 0.003 mol/L with constant stirring for 10 min at 60.0 °C [29]. A pale blue color developed in the solution after ten minutes. In a microwave oven (Panasonic N-ST342, Seoul, Republic of Korea), the mixture was irradiated for 5 min at 90.0 °C under an N_2 atmosphere. Pale blue turned into light brown in less than a minute. A 15 min centrifuge with three 5 min intervals was used to separate the CuO NPs from the solvent, followed by numerous washes with ethanol and also deionized water. Centrifugation caused the CuO NPs to sediment after washing and was followed by sonication in water for one minute. A refrigerator was used to store the CuO NPs after they were dried for 24 h at 400.0 °C. It was highly probable that CuO nanoparticles would form NPs when exposed to air. AP extract was an efficient reducing agent as well as a stabilizing agent in the formation of NPs.



Scheme 1. Synthesis of bio-reduced CuO NPs.

2.4. Antibacterial Activity

2.4.1. In-Vitro Antibacterial Efficacy

The assessment of the antibacterial efficacy of CuO NPs was performed using the agar well diffusion method [30]. For this study, *E. coli* as Gram-negative bacteria (ATCC 43895) and *S. aureus* as Gram-positive bacteria (ATCC 6538) were used. Briefly, on sterile Mueller Hinton agar (MHA) plates, overnight cultures of each bacterial strain at 0.5 McFarland standard were spread, which were pierced with a 7 mm diameter cork borer and loaded up with 50.0 μ L of CuO NPs diluted in 1.0% DMSO at different concentrations (10.0 μ g/mL, 200.0 μ g/mL, and 300.0 μ g/mL (*w/v*)). After the incubation process, the radius of the inhibition zone was measured by the use of a Vernier caliper. Clinical Laboratory Standards Institute (CLSI) bacteria and Cation-adjusted Mueller–Hinton broth media were used in this study. For reliable findings and reproducibility, experiments were carried out using at least two different cultures.

2.4.2. Antibiofilm Potency of CuO NPs against Bacterial Pathogens

A biofilm experiment was carried out on 96-well microtiter plates using the crystal violet staining technique [31]. The initial turbidities of OD 0.05 ($\sim 10^6$ CFU mL⁻¹) for *S. aureus* and OD 0.1 ($\sim 10^6$ CFU mL⁻¹) for *E. coli* at 600.0 nm were inoculated into an LB culture media (final volume 300.0 μ L) with or without the CuO NPs and incubated for 24 h without shaking at 37.0 °C. The formation of biofilm was confirmed by staining with 0.1% crystal violet for 30 min and washed frequently with distilled water and then 95.0% ethanol was added to each well. The absorbance of each plate well was recorded at 570.0 nm using a spectramax 190 microplate reader equipped with a xenon flash lamp (Molecular device, San Jose, CA, USA). Biofilm assays were carried out with two independent cultures in triplicate.

2.4.3. Antibiofilm Potency of CuO NPs against Bacterial Pathogens

A biofilm observation of the CuO NPs against both Gram-positive and Gram-negative bacterial pathogens have been measured by CLSM, and the detailed procedure has been provided in the Supplementary Materials.

2.5. Instruments Used

The bio-reduced CuO NPs are characterized by analytical instruments, and details are provided in the Supplementary Materials.

3. Results and Discussion

3.1. Analysis of Bio-Reduced CuO NPs by DRS

Figure 1 shows the DRS spectrum of pure CuO NPs. DRS curves were measured by UV-VIS-NIR spectrophotometers. NPs exhibit absorption bands in the range of 365.0 nm [32]. At 560.0 nm, a peak was observed as a shoulder, which implies the existence of CuO on the surface of NPs [32]. Furthermore, there was a weak reflectance in both the UV and visible ranges (200.0–800.0 nm). It also provided information about the greater absorption in the regions, as it gives weak transmittance. The band gap for the NPs was also calculated from the spectra and the value was 1.58 eV. The bandgap energy was higher than the bulk CuO material [33] and very close to the synthesized CuO NPs [34,35]. In the results, it consists only of CuO NPs and not of Cu.

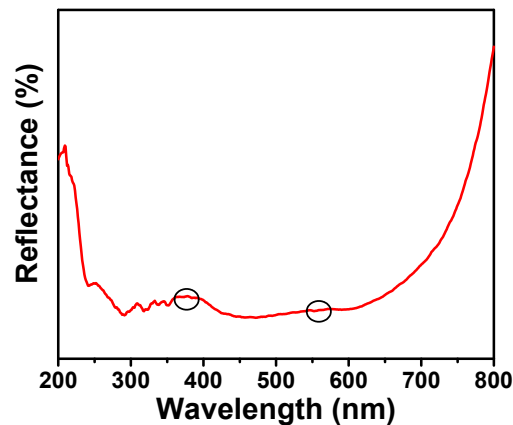


Figure 1. DRS spectra of bio-reduced CuO NPs.

3.2. Analysis of Bio-Reduced CuO NPs by FT-IR Spectrum

The effects of the peel extract used in the synthesis of NPs were analyzed by FT-IR analysis to obtain the structural and chemical properties of the synthesized metal oxides [36,37]. FT-IR spectra were recorded between 400.0 and 4000.0 cm^{-1} (Figure 2). CuO NPs have a peak at 3416.0 cm^{-1} , which was correlated with hydroxyl group stretching. NPs have a peak at 1650 cm^{-1} caused by a bending O–H. Another peak at 1376.0 cm^{-1} was related to C–O asymmetry in NPs. Another peak in the structure was at 1115.0 cm^{-1} , which was related to C–O symmetry. A peak at 533.0 cm^{-1} was associated with Cu–O bonds. There were three characteristic bands of CuO including the A_u mode, and two B_u modes of CuO appeared at 432.3 cm^{-1} , 497.0 cm^{-1} , and 603.3 cm^{-1} , respectively [38]. The high-frequency mode can be observed at 603.3 cm^{-1} and it has been attributed to the Cu–O stretching vibration in the [101] direction. The [101] direction of the Cu–O stretching vibration has been linked to the other peak, which can be seen at 497.0 cm^{-1} [39]. Therefore, the FT-IR analysis indicates that CuO NPs are in their pure phase and have a monoclinic structure.

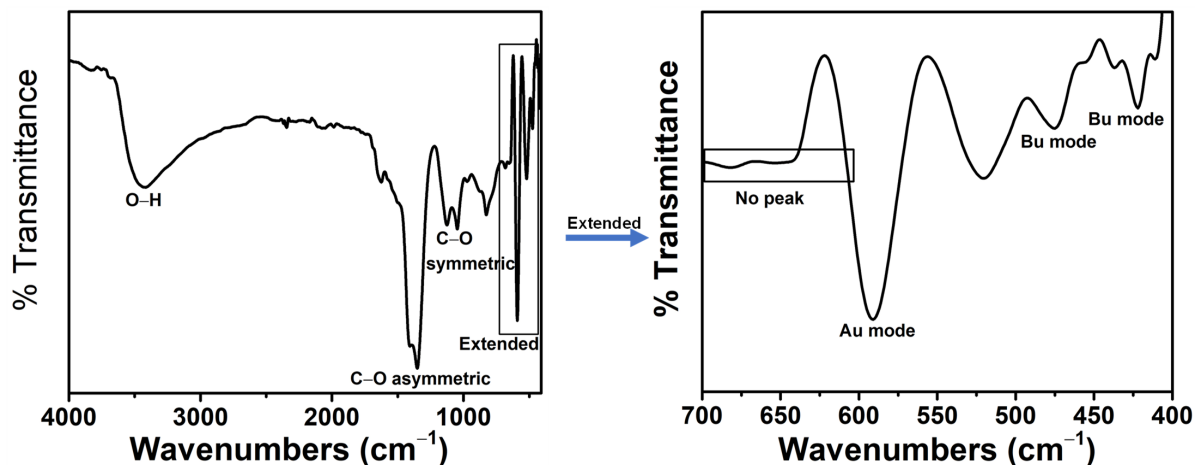


Figure 2. FT-IR spectrum of bio-reduced CuO NPs.

3.3. Analysis of Bio-Reduced CuO NPs by Raman Spectrum

Raman spectral analysis can be used as a major analytical technique to identify the vibrations of metal oxide NPs and local atomic arrangements and analyze their structural features [40,41]. It can also be used to determine how crystalline the NPs are. Figure 3 shows a strong peak at 283.0 cm^{-1} , which is associated with the A_g mode of vibration. The weak peaks that appeared at 312.0 cm^{-1} and 612.0 cm^{-1} corresponded to the B_g modes of vibration [41,42]. Only vertically and with a displacement do oxygen atoms move to the b-axis in Raman modes for both the A_g and B_g bands. Decreasing the size of the NPs altered a Raman shift and bandwidth [42].

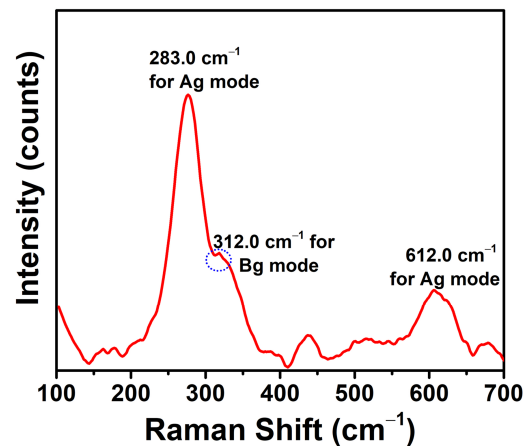


Figure 3. Raman spectra of bio-reduced CuO NPs.

3.4. Analysis of Bio-Reduced CuO NPs by XRD

Analysis of NPs obtained from metal oxides by XRD patterns is a powerful analytical technique to obtain information about the crystalline peaks [43]. Figure 4 shows the XRD patterns of CuO NPs at 2θ ranges from 20 to 80 (in degrees). According to the Joint Committee on Powder Diffraction Standards (JCPDS) database, crystalline phases were recognized. The patterns of NPs exhibited a significant peak at (2θ) 25.41, 32.51, 35.52, 38.32, 40.10, 42.51, 48.62, 53.10, 58.68, 61.52, and 62.64 (JCPDS01-080-1268) which belong to miller indices [021], [110], [002], [200], [130], [131], [202], [020], [002], [113], and [311], respectively [44,45]. Furthermore, there were some low-intensity peaks which may be due to the negligible amount of impurities in the NPs. Slight variations were observed in the obtained peaks at their position with respect to the JCPDS data, which may be due to the slight modifications in terms of phase on the surfaces of NPs. A strong intensity peak at 35.52 and a low-intensity peak at 38.32 appeared which revealed the formation of CuO and existed as the monoclinic phase [46]. Additionally, the sharp XRD patterns were evident for the crystalline nature as well as the monoclinic phase of the CuO on the whole surface of NPs. The lattice parameters a , b , and c were found to be 4.68 Å, 3.41 Å, and 5.08 Å, respectively. The average crystalline size was found to be 41.6 nm for the NPs according to the well-known Scherrer equation as follows [46,47],

$$D = (K\lambda)/(\beta \cdot \cos\theta) \quad (1)$$

where D stands for crystallite size (nm); K stands for Scherrer's constant that is associated with crystallite shape, normally taken as 0.9; β is the full width half maximum (radians), λ is the wavelength of the Cu $K\alpha$ radiation (1.54 Å); and θ is the Bragg angle (Å).

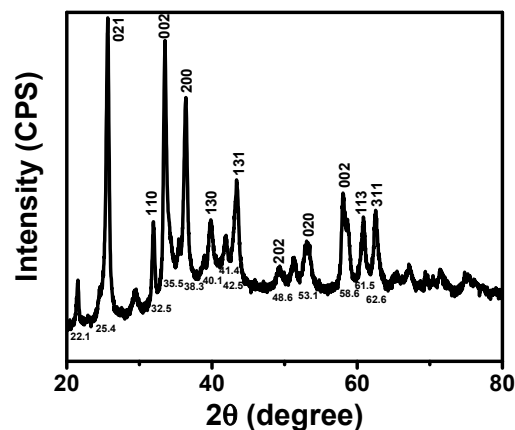


Figure 4. XRD patterns of bio-reduced CuO NPs.

3.5. Analysis of Bio-Reduced CuO NPs by FE-SEM

FE-SEM images were used for visual examination and analysis of the surface morphology of the NPs. An FE-SEM image of CuO NPs at different magnifications can be seen in Figure 5A–D. The CuO NPs were regular in shape with a particle-like structure. CuO NPs have particle sizes ranging from 25.0 to 55.0 nm and uniform distributions. Images show some particles with square shapes and clusters that have agglomerated together. Stabilized NPs can also form clusters of material-like particles relatively close together. The NPs were stabilized and reduced by the peel extract, allowing them to be re-dispersed [48]. A peel extract limits clustering and flocculation in order to control particle size distribution. In order to fabricate nanoparticles within the ranges of small sizes, apple peel extract was found to be an effective stabilizing agent. As a result, the assembly of NPs was found by processes of aggregation, growth of particles, and also impurity adsorption [49]. EDX results of the synthesized NPs confirm their chemical composition and particle distribution of NPs on the whole surface. The existence of Cu and O in the NPs is demonstrated in Figure 5E. Thus, the only two components of synthesized NPs were copper and oxygen. The pattern made it clear that the NPs are crystalline structures made of two elements, such as Cu and O. Solid and strong signals were observed around 0.92 keV, 8.05 keV, and 8.91 keV for Cu with Cu La, Cu Ka, and Cu Kb representations, respectively, and 0.53 keV for O with O Ka representation [50,51]. In Figure 5G,H, the elemental map of CuO NPs shows homogeneous distributions of Cu and O, respectively. It was confirmed by EDX elemental analysis that Cu and O were present in a single particle, with an atomic percent composition of Cu at 64.19% and O at 35.81%. Due to the coating of the carbon with the NPs to measure the SEM analysis, it was not considered for the composition of elements present in the NPs. It was confirmed by these results that a CuO structure can be formed within five minutes through microwave synthesis.

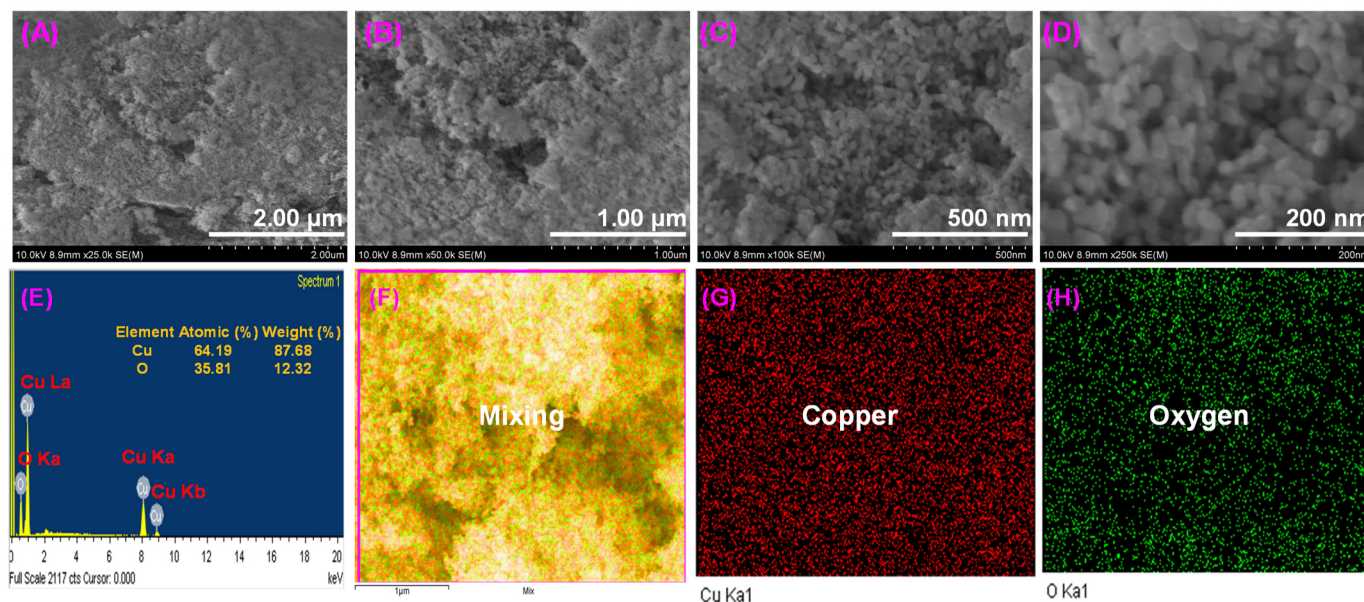


Figure 5. FE-SEM images of bio-reduced CuO NPs (A–D), EDX spectrum of bio-reduced CuO NPs (E), elemental mapping with mixing (F), elemental mapping of Cu (G), and elemental mapping of O (H).

3.6. Analysis of Bio-Reduced CuO NPs by HR-TEM

Figure 6A–E show HR-TEM images of the obtained CuO NPs with 31 nm scale bars. These TEM images and their SAED patterns indicate the size and crystallinity of the NPs [52,53]. These images show spherical NPs with an average diameter of 40.2 ± 4.0 nm and a narrow distribution of particle sizes. Analyses of particle size distributions were performed using ImageJ software. Due to NP agglomeration, spherical nature, and in-

terconnections, Figure 6 closely matches SEM results. According to Figure 6F, the SAED pattern corresponds to the BCC crystalline structure of CuO, indexed to planes (021), (110), (002), (200), (130), (131), (202), (020), (002), (113), and (311). The spacing of the lattice fringes in one direction was about 0.21 nm. Morphological characterization of the NPs using FE-SEM and HR-TEM revealed that they were agglomerated.

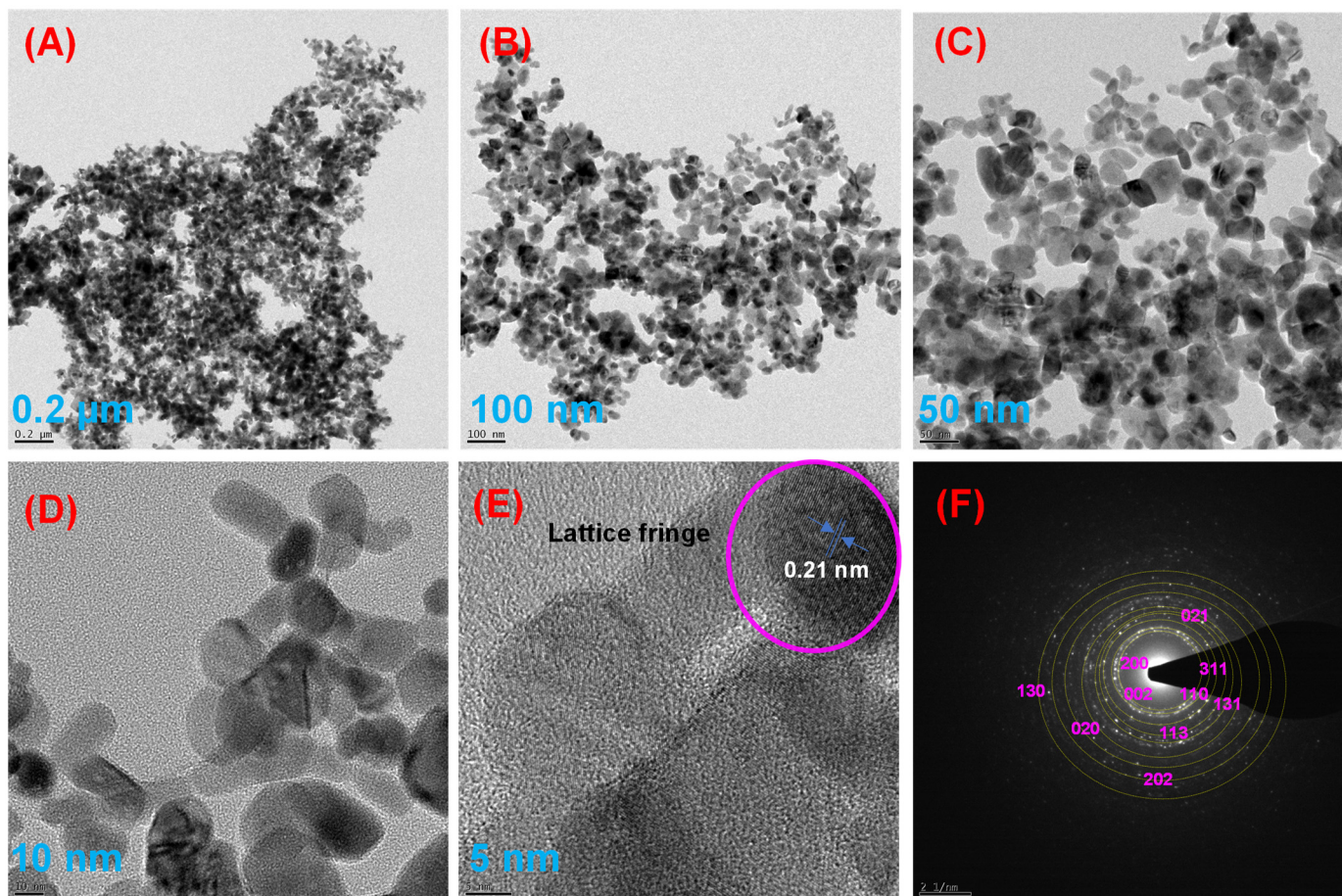


Figure 6. HR-TEM images of bio-reduced CuO NPs (A–E); SAED patterns of bio-reduced CuO NPs (F).

3.7. Analysis of Bio-Reduced CuO NPs by XPS

CuO NPs were analyzed using XPS analysis—a powerful surface-sensitive technique for the determination of oxidation state as well as chemical composition in the NPs [54]. For the standardization of all binding energies, the C 1s peak that appeared at 284.60 eV was used as a reference. According to Figure 7A, the peaks of the XPS wide scan spectrum were associated with Cu, C, and O elements. According to Figure 7B–D, the XPS spectra of Cu 2p, C 1s, and O 1s were measured with high-resolution (core XPS) spectra. The narrow energy range spectra of Cu 2p demonstrated a predominant peak at the stronger binding side of Cu 2p_{3/2} and increased binding energy, indicating an unfilled Cu 3d₉ shell. The presence of Cu²⁺ in the CuO sample [55] was further confirmed by the presence of an unfilled Cu 3d₉ shell. Additionally, the peaks at 953.28 eV and 933.38 eV in the core level spectrum of Cu 2p (deconvolution of CuO NPs, Figure 7B) can be attributed to two possibilities, such as Cu 2p_{3/2} and Cu 2p_{1/2} of CuO NPs, respectively. A high-resolution spectrum of carbon (C 1s) is shown in Figure 7C, which confirms the reference peak at 284.48 eV and other higher energy peaks at 286.08 eV and 288.41 eV. As a charge reference for the XPS spectra on the surface of NPs, the three peaks of the C 1s spectrum were known as contamination of adventitious carbon. The first peak of C 1s had a binding energy of

284.67 eV, indicating adventitious carbon containing the C–C bond; the second peak of C 1s had a binding energy of 286.08 eV, indicating adventitious carbon containing the C–O–C bond; and the third peak of C 1s had a binding energy of 288.08 eV, indicating adventitious carbon containing O–C=O bonds. According to the Gaussian–Lorentzian fit of O1s, two components were present at 529.08 eV and 530.88 eV (Figure 7D). This peak at 529.08 eV was attributed to the binding energy of lattice oxygen (O_L)^{2−} in CuO lattices and agrees with $O^{2−}$ in metal oxides ($Cu^{2+} - O^{2−}$) [56]. It can be determined that the second peak at 530.88 eV reflects the binding energy for the oxygen vacancies or defects within the environment of CuO NPs [57]. According to the XPS spectra of NPs, there was no possibility of residual nitrogen in the precursor. As a result of measuring the XPS spectrum, CuO NPs were verified to be structurally stable.

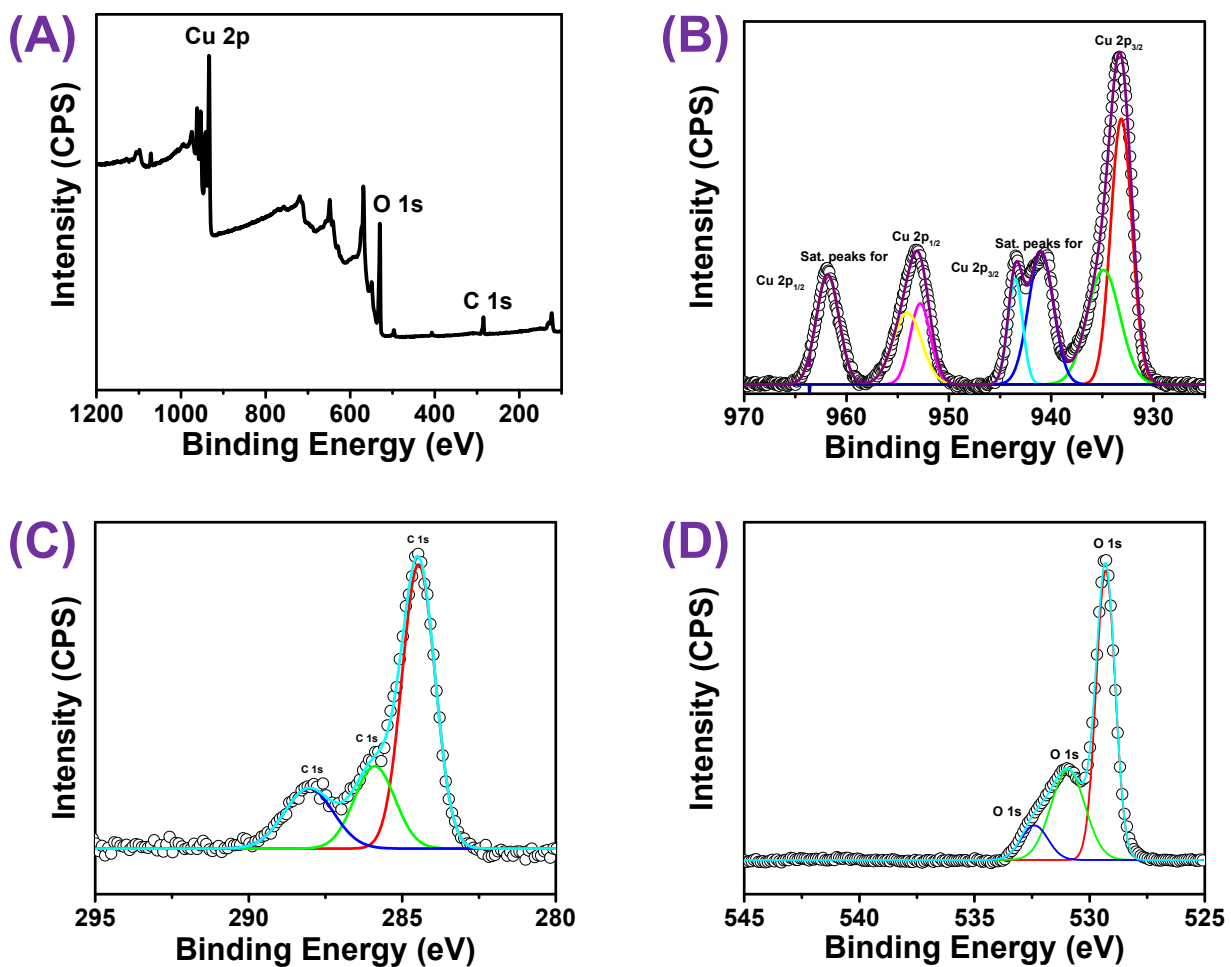


Figure 7. XPS of (A) survey scan spectrum, (B) Cu 2p, (C) C 1s, and (D) O 1s.

3.8. Analysis of Bio-Reduced CuO NPs by TG/DTA

The thermal stability of the NPs was typically evaluated using the TG/DTA curves, and a weight loss (in%) can be determined in relation to an increase in temperature [58]. The TGA and DTA curves of CuO NPs are displayed in Figure 8. The exothermic peak in the DTA curves at 201.9 °C indicated the release of energy from the surface of NPs into the surrounding environment. There was not much weight loss observed in the ranges of 30.0–800.0 °C [59]. However, the weight loss percentage was very little at three stages of temperatures, 110.0–210.0 °C, 300.0–410.0 °C, and 670.0–800.0 °C. The above three weight stages were mainly due to the release of moisture content and peel extract from the surface of NPs, as desorption had taken place during the thermal analysis [60]. Thus, the NPs were very stable up to 800.0 °C without decomposition.

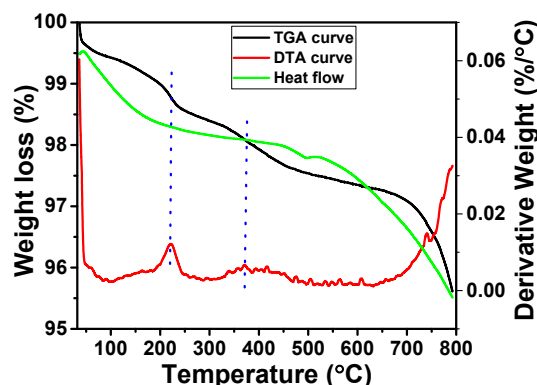


Figure 8. TGDTA curves of bio-reduced CuO NPs.

3.9. Analysis of Bio-Reduced CuO NPs by BET Surface Area

The pore size distribution and surface area of CuO NPs were studied using N_2 gas adsorption with BET surface area analysis. The adsorption–desorption curve follows a type IV isotherm obtained for the CuO NPs and is shown in Figure 9A. The hysteresis loop within the relative pressure (P/P_0) ranges from 0.7 to 0.9 confirmed the presence of the mesoporous nature of the obtained NPs [61]. The surface areas were calculated to be $31.8240 \text{ m}^2/\text{g}$ by the standard multi-point BET (Figure 9B). The pore-size distribution was investigated for the obtained NPs by the desorption of the BJH method [62,63]. The pore size value was found to be 39.19 nm, which was clearly shown in Figure 9C, D. The results of pore size and surface area are consolidated in Table 1. Thus, the pore size shows that the NPs are mesoporous in nature which matched well with the porosity results obtained from the XRD analysis, FESEM, and also HRTEM images.

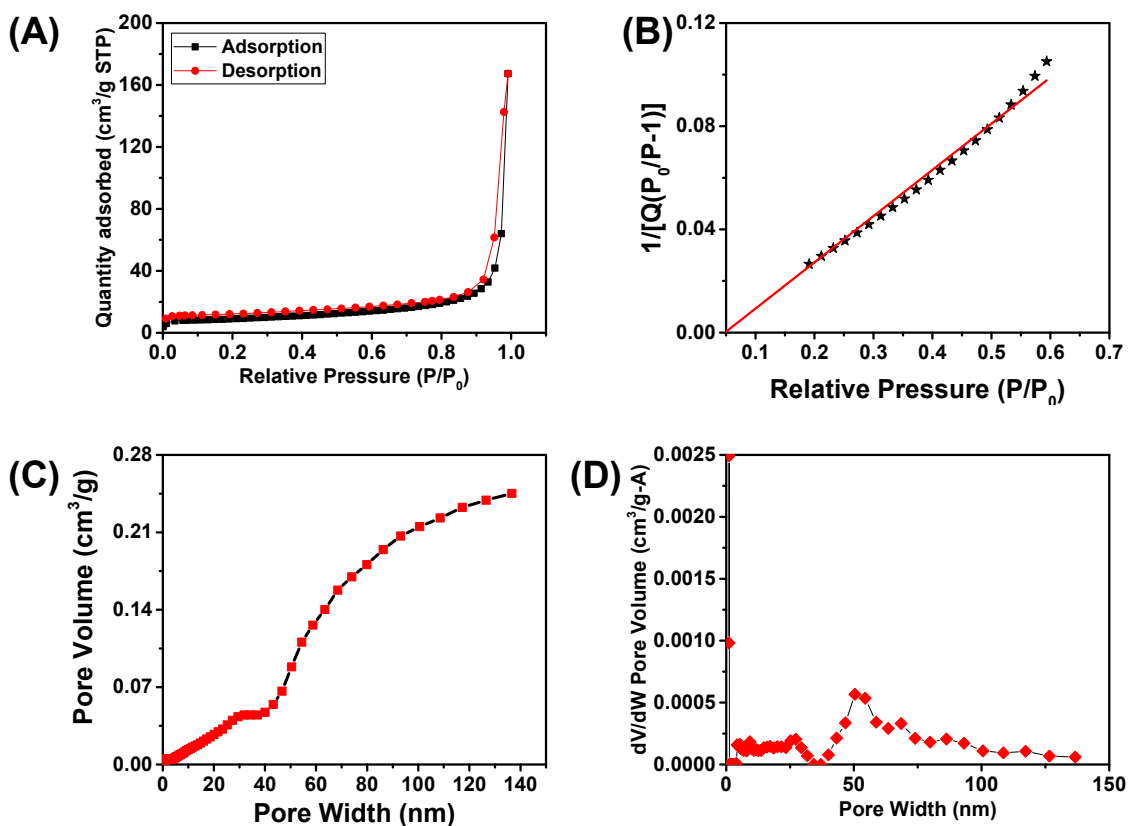


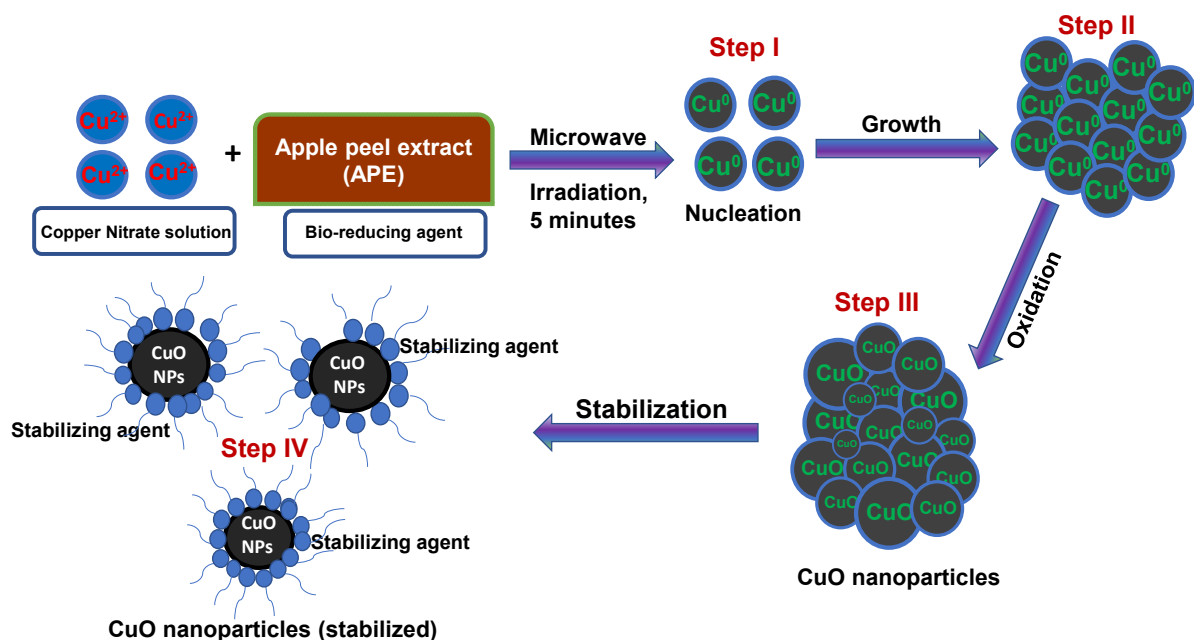
Figure 9. BET surface analysis with N_2 gas adsorption–desorption isotherms of bio-reduced CuO NPs (A), surface area plot (B), BJH desorption pore size distribution (C), and differential pore volume plot (D).

Table 1. Surface area, pore volume, and pore size distribution of CuO NPs by BET analysis.

Material	Surface Area (m ² /g)	Pore Volume (m ³ /g)			Pore Size (nm)	
		t-Plot Micropore Volume	BJH Adsorption Cumulative Volume of Pores	BJH Desorption Cumulative Volume of Pores	BJH Adsorption Average Pore Diameter (4V/A)	BJH Desorption Average Pore Diameter (4V/A)
CuO NPs	31.8240	0.005294	0.255223	0.251015	42.44	39.19

3.10. A Probable Mechanism of Bio-Reduced CuO NPs

An outline of the suggested CuO NPs mechanism is given in Scheme 2. As part of the biosynthetic process, there were usually three processing stages, which include the activation, growth, and termination phases [64,65]. In this process, the extract may act as a reducing as well as a stabilizing agent. In an initial step, a CuNO₃·2H₂O salt precursor would be dissolved in distilled water and activated by removing its cations. Copper ions and AP extract undergo an oxidation–reduction reaction during mixing. Cationic copper was reduced and the oxidation state became 2+ into a metallic form. The nucleation process (Cu⁰) involves the direct conversion of electron-rich natural constituents (AP extract as a bio-reducing agent) directly into CuO NPs due to the greater chemical reactivity on their surfaces. The hydroxyl group of the AP extract effectively participated in the reducing process, and as evident in Figure 2, a broad peak is visible at 3416.0 cm^{−1} for the hydroxyl groups in the AP extract. During the oxidation process, the Cu⁰ was progressively combined and the growth of CuO NPs commenced [66]. In the third stage, CuO NPs were stabilized. A strong protective shield layer formed and it surrounded the entire surface of the nucleated NPs; hence, limiting the growth of NPs. Additionally, these extracts use steric pressures to keep the capped NPs apart [67]. Similarly, food waste materials contain a variety of bioactive components that could aid in lowering metal ions or metal oxides as well as stabilizing metallic NPs [68].

**Scheme 2.** Schematic procedure for the bio-reduced CuO NPs [62].

3.11. Antibacterial Efficacy of Bio-Reduced CuO NPs

Both Gram-positive and Gram-negative bacteria tested were susceptible to CuO NPs. *E. coli* and *S. aureus* were susceptible to NPs with MIC values of 50.0 µg/mL and MBC 100 µg/mL, respectively. Additionally, the agar diffusion test was carried out for the assessment of the antibacterial activity of CuO NPs and showed a clear zone for the

activity against both bacteria. The diameters of inhibition zones after the treatment are consolidated in Table 2 and representative images are shown in Figure 10. The results revealed that the zone of inhibition grew significantly with respect to the concentration of CuO NPs. There was a direct relationship between the zone of inhibition and the concentrations of NPs. In *E. coli* and *S. aureus*, the zone of inhibition was determined to be 29.0 ± 2.3 mm and 26.0 ± 1.1 mm, respectively. CuO NPs have been shown to be particularly effective against various types of bacterial strains [69]. The highly unique surface characteristics of CuO NPs to volume ratio permit them to interact across the surface of the cell membrane of the bacterial pathogen, finally killing the bacterial pathogen [70]. Particularly, electronic interactions, produced by CuO NPs with a smaller size and a larger surface area, were helpful to enhance the surface responsiveness of NPs. Additionally, the improved surface area percent instantly acts together with the bacterium, causing enhanced bacteria interaction during the process. These two crucial elements (Cu and O in NPs) play a significant role in enhancing the antibacterial efficacy of NPs with a large surface area [71].

Table 2. Antibacterial efficacy of bio-reduced CuO NPs at different concentrations against *S. aureus* and *E. coli* by a zone of inhibition.

Name of the Bacterial Strains	Zone of Inhibition (mm)			
	Conc. of CuO NPs ($\mu\text{g}/\text{mL}$)			
	300.0	200.0	100.0	0
<i>S. aureus</i>	26.0 ± 1.1	23.0 ± 1.3	19.0 ± 0.9	ND
<i>E. coli</i>	29.0 ± 2.3	26.0 ± 0.8	20.0 ± 0.5	ND

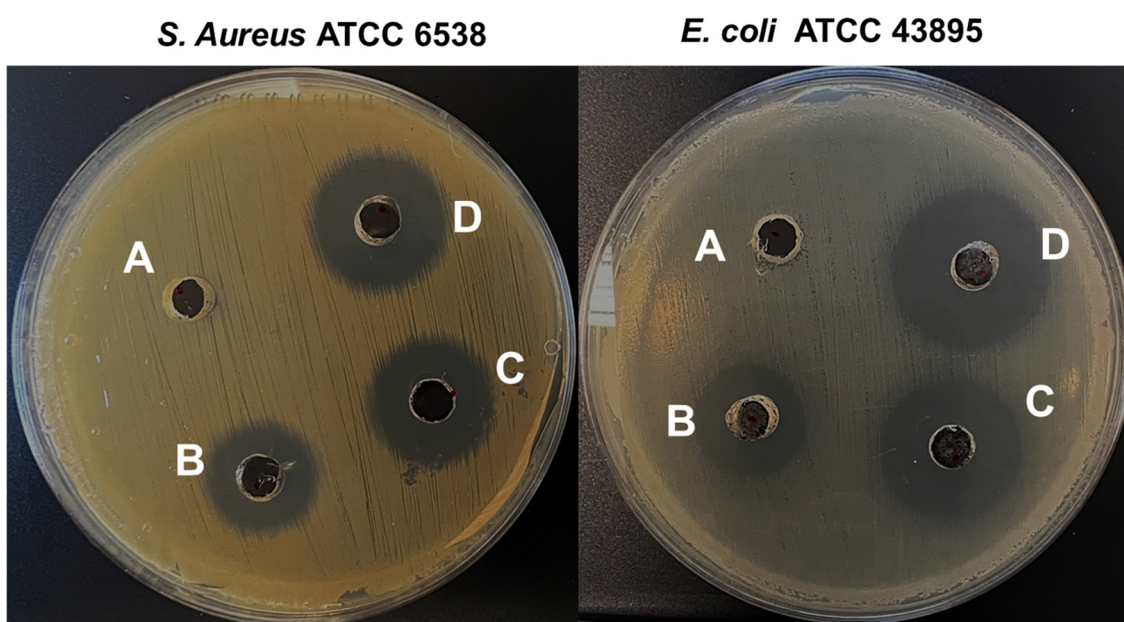


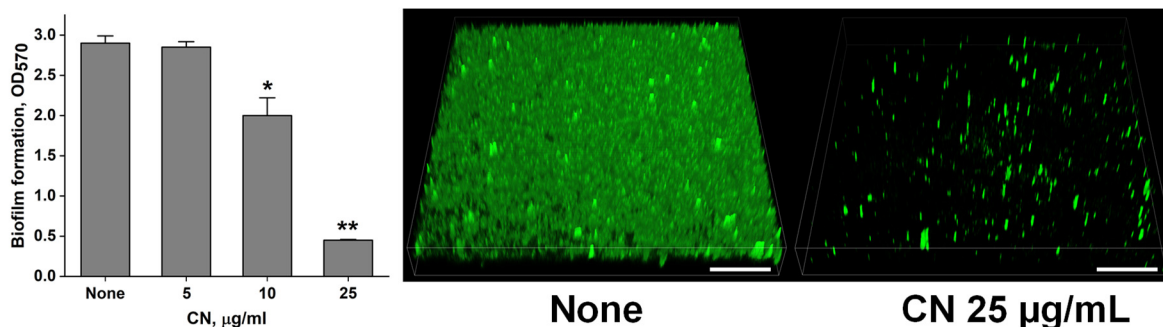
Figure 10. Antibacterial efficacy of bio-reduced CuO NPs with different concentrations (A, 0 $\mu\text{g}/\text{mL}$; B, 100 $\mu\text{g}/\text{mL}$; C, 200 $\mu\text{g}/\text{mL}$; and D, 300 $\mu\text{g}/\text{mL}$).

3.12. Antibiofilm Potency of Bio-Reduced CuO NPs against *E. coli* and *S. aureus*

A biofilm potency of NPs was performed against *E. coli* and *S. aureus*. Figure 11 shows the dose-dependent antibiofilm inhibition after the treatment with NPs at doses of 5.0 $\mu\text{g}/\text{mL}$, 10.0 $\mu\text{g}/\text{mL}$, and 25.0 $\mu\text{g}/\text{mL}$. As a result, NPs at a lower dose of 10.0 $\mu\text{g}/\text{mL}$ inhibited 12.0 ± 10.7 and $31.0 \pm 7.2\%$ biofilm formation by *E. coli* and *S. aureus* after 24 h of incubation, respectively. Furthermore, when the dose of NPs was increased to 25.0 $\mu\text{g}/\text{mL}$, significant inhibition of *E. coli* and *S. aureus* biofilm formation was observed $>60.0 \pm 2.3$

and $80.0 \pm 0.3\%$, respectively. The CuO-containing polymeric or non-polymeric NPs were reported to be antibacterial as well as antibiofilm (28.0 to 69.0%) agents against *E. coli* and *S. aureus* [69], *Bacillus subtilis*, and *Pseudomonas aeruginosa* [72]. In the current study, the synthesized NPs inhibited selective *E. coli* and *S. aureus* biofilm at lower concentrations, whereas as concentration increased the NPs showed potential antibacterial efficacy against both tested bacterial strains. Additionally, reduced biofilm thickness was confirmed by confocal laser microscopy (Figure 11) and COMSTAT biofilm analysis (Table 3). NPs at 25.0 $\mu\text{g}/\text{mL}$ reduced biomass and mean thickness of both pathogens, *E. coli* and *S. aureus*, by >65.0 and 85.0% , respectively, according to untreated controls (Table 3). From an applications point of view, CuO NPs are used in various industry sectors; moreover, there is a medical application of CuO NPs as antibacterial material [73]. Concerns are raised by their toxicity, which includes toxicity to the blood and immune system, but knowledge of their immunotoxicity is still relatively restricted. CuO NPs or material decorated with NPs prevents the growth of biofilm or adherent populations of microorganisms on the surface of materials [74]. Recently, Boliang et al. reported in 2022 that biosynthesized CuO NPs enhance antibiofilm activity against *K. pneumoniae* and *S. aureus* [75].

A *S. aureus* ATCC 6538



B *E. coli* ATCC 43895

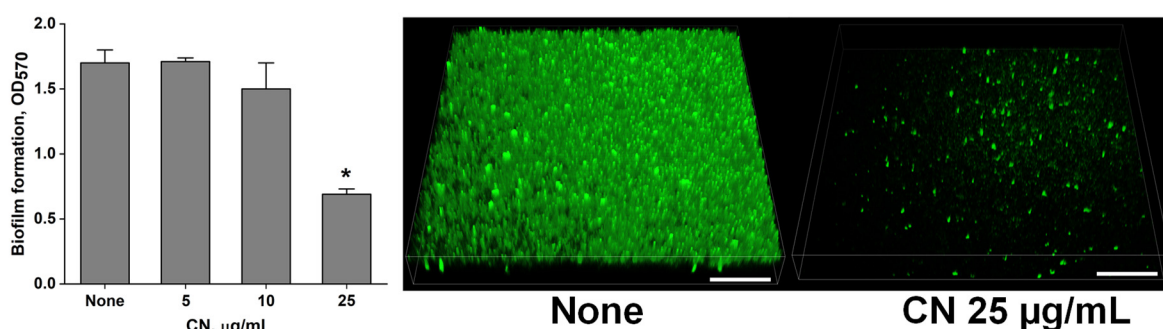


Figure 11. Effects of bio-reduced CuO NPs on *S. aureus* (A) and *E. coli* (B) biofilm formation. ** $p < 0.01$ * $p < 0.05$ Vs. non-treated controls. Scale bars represent 100.0 μm .

Table 3. COMSTAT analysis of biofilm biomass, mean thickness, and substratum coverage spatial characteristics.

Bacterial Strains	Biofilm Biomass ($\mu\text{m}^3 \mu\text{m}^{-2}$)		Mean Thickness (μm)		Substratum Coverages (%)	
	None	25.0 $\mu\text{g}/\text{mL}$	None	25.0 $\mu\text{g}/\text{mL}$	None	25.0 $\mu\text{g}/\text{mL}$
<i>S. aureus</i>	43.02 ± 2.4	6.11 ± 0.6	46.38 ± 3.1	11.36 ± 1.1	100 ± 0.8	8.01 ± 1.2
<i>E. coli</i>	40.80 ± 1.9	9.01 ± 1.0	39.42 ± 1.1	16.40 ± 0.4	100 ± 0.4	12.4 ± 2.1

4. Conclusions

For the quick one-pot production of CuO NPs, pressure control or a higher temperature was not necessary to maintain. The XRD pattern revealed that all of the NPs had a monoclinic crystalline structure. According to XPS and EDX studies, Cu and O make up the NPs. The pore-size distribution was investigated for the obtained NPs by the desorption of the BJH method, which revealed that the NPs are mesoporous in nature. The pore size for the NPs was found to be 39.19 nm. An in vitro antibacterial efficacy of CuO NPs was tested against the bacterial pathogens *E. coli* and *S. aureus*. The results revealed a clear zone of inhibition against both bacterial strains. The highly unique surface characteristics of CuO NPs to volume ratio enable them to interact across the surface of the bacterial cell membrane eventually leads to killing them. A biofilm assay was also performed to examine the antibiofilm potency of NPs against both pathogens. NPs at 25.0 µg/mL reduced the biomass and mean thickness of both the bacterial pathogens by >85.0% and 65.0%, with respect to the untreated controls. In the near future, disease detection may be the primary focus of CuO NPs' biological uses; however, they may also have potential applications in a wide range of other fields.

Supplementary Materials: The following supporting information can be downloaded at: <https://www.mdpi.com/article/10.3390/ma16010217/s1>; the preparation of extract, biofilm observations by confocal laser scanning microscopy, and instruments used for the characterization of CuO NPs are provided in the Supplementary Materials.

Author Contributions: Conceptualization, methodology, interpretation, and writing—original draft, R.R.: methodology, interpretation, and writing—original draft, C.J.R.: review and editing, S.-C.K.: review, editing, and supervision, Y.R.L. All authors have read and agreed to the published version of the manuscript.

Funding: This research received no external funding.

Institutional Review Board Statement: Not applicable.

Informed Consent Statement: Not applicable.

Data Availability Statement: The datasets used or analyzed during the current study are available from the corresponding author upon reasonable request.

Conflicts of Interest: The authors declare no conflict of interest.

References

1. Myrna, R.-B.; Nadja, M.M.-L.; Carla, M.R.-Q.; Ana, L.V.-A.; Felix, R.R.-V.; Oscar, J.P.-P. Single Step Microwave Assisted Synthesis and Antimicrobial Activity of Silver, Copper and Silver-Copper Nanoparticles. *J. Mater. Sci. Chem. Eng.* **2020**, *8*, 13–29.
2. CDC. Annual Summaries of Foodborne Outbreaks | Foodborne Outbreak Surveillance System. Food Safety. 2017. Available online: <https://www.cdc.gov/fdoss/annual-reports/index.html> (accessed on 31 December 2017).
3. CDC. Foodborne Germs and Illness. 2020. Available online: <https://www.cdc.gov/foodsafety/foodborne-germs.html> (accessed on 31 December 2020).
4. Beyth, N.; Hourri-Haddad, Y.; Domb, A.; Khan, W.; Hazan, R. Alternative Antimicrobial Approach: Nano-Antimicrobial Materials. *Evid.-Based Complement. Altern. Med.* **2015**, *2015*, 246012. [[CrossRef](#)] [[PubMed](#)]
5. Das, B.; Dash, S.K.; Mandal, D.; Ghosh, T.; Chattopadhyay, S.; Tripathy, S. Green Synthesized Silver Nanoparticles Destroy Multidrug Resistant Bacteria via Reactive Oxygen Species Mediated Membrane Damage. *Arab. J. Chem.* **2017**, *10*, 862–876. [[CrossRef](#)]
6. Sharif, Z.; Mustapha, F.J.Y. Revisión de métodos de preservación y conservantes naturales para extender la longevidad de los alimentos. *Ing. Quim.* **2017**, *19*, 145–153.
7. Molkenova, A.; Sarsenov, S.; Atabaev, S.; Khamkhash, L.; Atabaev, T.S. Hierarchically-structured hollow CuO microparticles for efficient photo-degradation of a model pollutant dye under the solar light illumination. *Environ. Nanotechnol. Monit. Manag.* **2021**, *16*, 100507. [[CrossRef](#)]
8. Ambardekar, V.; Sahoo, S.; Srivastava, D.K.; Majumder, S.B.; Bandyopadhyay, P.P. Plasma sprayed CuO coatings for gas sensing and catalytic conversion applications. *Sens. Actuators B* **2021**, *331*, 129404. [[CrossRef](#)]
9. Vasantharaj, S.; Sathiyavimal, S.; Senthilkumar, P.; Oscar, F.L.; Pugazhendhi, A. Biosynthesis of iron oxide nanoparticles using leaf extract of *Ruellia tuberosa*: Antimicrobial properties and their applications in photocatalytic degradation. *J. Photochem. Photobiol. B* **2019**, *192*, 74–82. [[CrossRef](#)]

10. Pramanika, A.; Laha, D.; Chattopadhyay, S.; Dash, S.; Roy, S.; Pramanik, P.; Karmakar, P. Targeted delivery of chitosan-Folic acid coated “copper carbonate” nanoparticle to cancer cells in-vivo. *Toxicol. Res.* **2015**, *4*, 1604–1612. [[CrossRef](#)]
11. Laha, D.; Pramanik, A.; Maity, J.; Mukherjee, A.; Pramanik, P.; Karmakar, P. Interplay between autophagy and apoptosis mediated by copper oxide nanoparticles in human breast cancer cells MCF7. *Biochim. Biophys. Acta* **2014**, *1840*, 1–9. [[CrossRef](#)]
12. Maqbool, Q.; Iftikhar, S.; Nazar, M.; Abbas, F.; Saleem, A.; Hussain, T.; Kausar, R.; Anwaar, S.; Jabeen, N. Green fabricated CuO nanobullets via *Olea europaea* leaf extract shows auspicious antimicrobial potential. *IET Nanobiotechnol.* **2017**, *11*, 463–468. [[CrossRef](#)]
13. Mohammed, W.M.; Mubark, T.H.; Al-Haddad, R.M.S. Effect of CuO nanoparticles on antimicrobial activity prepared by sol-gel method. *Int. J. Appl. Eng. Res. Dev.* **2018**, *13*, 10559–10562.
14. Akhavan, O.; Ghaderi, E. Cu and CuO nanoparticles immobilized by silica thin films as antibacterial materials and photocatalysts. *Surf. Coat. Technol.* **2010**, *205*, 207–213. [[CrossRef](#)]
15. Heinlaan, M.; Ivask, A.; Bilnova, I.; Dubourguier, H.C.; Kahru, A. Toxicity of nanosized and bulk ZnO, CuO and TiO₂ to bacteria *Vibrio fischeri* and crustaceans *Daphnia magna* and *Thamnocephalus platyurus*. *Chemosphere* **2008**, *71*, 1308–1316. [[CrossRef](#)] [[PubMed](#)]
16. Akintelu, S.A.; Folorunso, A.S.; Folorunso, F.A.; Oyebamiji, A.K. Green synthesis of copper oxide nanoparticles for biomedical application and environmental remediation. *Heliyon* **2020**, *6*, e04508. [[CrossRef](#)] [[PubMed](#)]
17. Rania, D.; Rabah, A.; Mamadou, T.; Christine, M.; Andrei, K. Antibacterial activity of ZnO and CuO nanoparticles against gram positive and gram negative strains. *Mater. Sci. Eng. C* **2019**, *104*, 109968.
18. Ameer, A.; Arham, S.A.; Oves, M.; Khan, M.S.; Adnan, M. Size-dependent antimicrobial properties of CuO nanoparticles against Gram-positive and -negative bacterial strains. *Int. J. Nanomed.* **2012**, *7*, 3527–3535.
19. Hina, Q.; Sumbul, R.; Dushyant Kumar, C.; Ashok Kumar, T.; Vikramaditya, U. Green Synthesis, Characterization and Antimicrobial Activity of Copper Oxide Nanomaterial Derived from *Momordica charantia*. *Int. J. Nanomed.* **2020**, *15*, 2541–2553.
20. Jeronsia, J.E.; Joseph, L.A.; Vinosha, P.A.; Mary, A.J.; Das, S.J. *Camellia sinensis* leaf extract mediated synthesis of copper oxide nanostructures for potential biomedical applications. *Mater. Today Proc.* **2019**, *8*, 214–222. [[CrossRef](#)]
21. Koupaei, M.H.; Shareghi, B.; Saboury, A.A.; Davar, F.; Semnani, A.; Evini, M. Green synthesis of zinc oxide nanoparticles and their effect on the stability and activity of proteinase K. *RSC Adv.* **2016**, *6*, 42313–42323. [[CrossRef](#)]
22. Awwad, A.M.; Albiss, B.A.; Salem, N.M. Antibacterial activity of synthesized copper oxide nanoparticles using malva sylvestris leaf extract. *SMU Med. J.* **2015**, *2*, 91–101.
23. Pugazhendhi, A.; Kumar, S.S.; Manikandan, M.; Saravanan, M. Photocatalytic properties and antimicrobial efficacy of Fe doped CuO nanoparticles against the pathogenic bacteria and fungi. *Microb. Pathog.* **2018**, *122*, 84–89. [[CrossRef](#)]
24. Vasantharaj, S.; Sathiyavimal, S.; Saravanan, M.; Senthilkumar, P.; Gnanasekaran, K.; Shanmugavel, M.; Manikandan, E.; Pugazhendhi, A. Synthesis of ecofriendly copper oxide nanoparticles for fabrication over textile fabrics: Characterization of antibacterial activity and dye degradation potential. *J. Photochem. Photobiol. B Biol.* **2019**, *191*, 143–149. [[CrossRef](#)]
25. Yang, N.; Weihong, L.; Hao, L. Biosynthesis of Au nanoparticles using agricultural waste mango peel extract and its in vitro cytotoxic effect on two normal cells. *Mater. Lett.* **2014**, *134*, 67–70. [[CrossRef](#)]
26. Yang, B.; Qi, F.; Tan, J.; Yu, T.; Qu, C. Study of green synthesis of ultrasmall gold nanoparticles using Citrus sinensis peel. *Appl. Sci.* **2019**, *9*, 2423. [[CrossRef](#)]
27. Gangapuram, B.R.; Bandi, R.; Alle, M.; Dadigala, R.; Kotu, G.M.; Guttena, V. Microwave assisted rapid green synthesis of gold nanoparticles using *Annona squamosa* L peel extract for the efficient catalytic reduction of organic pollutants. *J. Mol. Struct.* **2018**, *1167*, 305–315. [[CrossRef](#)]
28. Mahmoud, N.; Fatemeh, G.; Zahra, I.; Mohammad, S. Recent developments in the biosynthesis of Cu-based recyclable photocatalysts using plant extracts and their application in the chemical reactions. *Chem. Rec.* **2019**, *19*, 601–643.
29. He, X.; Liu, R.H. Phytochemicals of Apple Peels: Isolation, Structure Elucidation, and Their Antiproliferative and Antioxidant Activities. *J. Agric. Food Chem.* **2008**, *56*, 9905–9910. [[CrossRef](#)]
30. Mohamed, A.A.; Abu-Elghait, M.; Ahmed, N.E.; Salem, S.S. Eco-friendly mycogenic synthesis of ZnO and CuO nanoparticles for *in-vitro* antibacterial, antibiofilm, and antifungal applications. *Biol. Trace Elem. Res.* **2021**, *199*, 2788–2799. [[CrossRef](#)]
31. Kim, Y.-G.; Lee, J.-H.; Raorane, C.J.; Oh, S.T.; Park, J.G.; Lee, J. Herring Oil and Omega Fatty Acids Inhibit *Staphylococcus aureus* Biofilm Formation and Virulence. *Front. Microbiol.* **2018**, *9*, 1241. [[CrossRef](#)]
32. Junfei, F.; Yimin, X. Investigation of optical absorption and photothermal conversion characteristics of binary CuO/ZnO nanofluids. *RSC Adv.* **2022**, *7*, 56023–56033.
33. Mohammad, S.D.; Mostafa, Z.M. Experimental study of water-based CuO nanofluid flow in heat pipe solar collector. *J. Therm. Anal. Calorim.* **2019**, *137*, 2061–2072.
34. Maji, S.K.; Mukherjee, N.; Mondal, A.; Adhikary, B.; Karmakar, B. Chemical synthesis of mesoporous CuO from a single precursor: Structural, optical and electrical properties. *J. Solid State Chem.* **2010**, *183*, 1900–1904. [[CrossRef](#)]
35. Lin, H.-H.; Wang, C.-Y.; Shih, H.C.; Chen, J.-M.; Hsieh, C.-T. Characterizing well-ordered CuO nanofibrils synthesized through gas-solid reactions. *J. Appl. Phys.* **2004**, *95*, 5889–5895. [[CrossRef](#)]
36. Kaur, M.; Muthe, K.P.; Deshpande, S.K.; Shipra, C.; Singh, J.B.; Neeika, V.; Gupta, S.K.; Yakh-mi, J.V. Growth and branching of CuO nanowires by thermal oxidation of copper. *J. Cryst. Growth* **2006**, *289*, 670–675. [[CrossRef](#)]

37. Anita, S.E.; Dae, J.K. Synthesis and characterization of CuO nanowires by a simple wet chemical method. *Nanoscale Res. Lett.* **2012**, *7*, 70.
38. Nyquist, R.A.; Kagel, R.O. *Infrared Spectra of Inorganic Compounds*; Academic Press: New York, NY, USA; London, UK, 1997; Volume 220.
39. Kliche, K.; Popovic, Z.V. Far-infrared spectroscopic investigations on CuO. *Phys. Rev. B* **1990**, *42*, 10060–10066. [[CrossRef](#)]
40. Benhammada, A.; Trache, D.; Chelouche, S.; Mezroua, A. Catalytic Effect of green Cu₂O nanoparticles on the thermal decomposition kinetics of ammonium perchlorate. *Z. Anorg. Allg. Chem.* **2021**, *647*, 312–325. [[CrossRef](#)]
41. Karthikeyan, B. Raman spectral probed electron–phonon coupling and phonon lifetime properties of Ni-doped CuO nanoparticles. *Appl. Phys. A* **2021**, *127*, 205. [[CrossRef](#)]
42. Angeline Mary, A.P.; Thaminum Ansari, A.; Subramanian, R. Sugarcane juice mediated synthesis of copper oxide nanoparticles, characterization and their antibacterial activity. *J. King Saud Univ. Sci.* **2019**, *31*, 1103–1114. [[CrossRef](#)]
43. Saad, N.A.; Dar, M.H.; Ramya, E.; Naraharisetty, S.R.G.; Narayana Rao, D. Saturable and reverse saturable absorption of a Cu₂O-Ag nanoheterostructure. *J. Mater. Sci.* **2019**, *54*, 188–199. [[CrossRef](#)]
44. Nagajyothi, P.; Muthuraman, P.; Sreekanth, T.; Kim, D.H.; Shim, J. Green synthesis: In-vitro anticancer activity of copper oxide nanoparticles against human cervical carcinoma cells. *Arab. J. Chem.* **2017**, *10*, 215–225. [[CrossRef](#)]
45. Chandan, T.; Indranirekha, S.; Moushumi, H.; Manash, R.D. Reduction of aromatic nitro compounds catalyzed by biogenic CuO nanoparticles. *RSC Adv.* **2014**, *4*, 53229–53236.
46. Ehsan, A.; Mohammad, H.; Reza, S.; Maryam, S. Copper plasmon-induced Cu-doped ZnO-CuO double-nanoheterojunction: In-situ combustion synthesis and photo-decontamination of textile effluents. *Mater. Res. Bull.* **2020**, *129*, 110880.
47. Masoud, M.; Abdullah, I.; Reza, I. A performance study on the electrocoating process with CuZnAl nanocatalyst for a methanol steam reformer: The effect of time and voltage. *RSC Adv.* **2016**, *6*, 25934–25942.
48. Qiuli, Z.; Zhimao, Y.; Bingjun, D.; Xinzhe, L.; Yingjuan, G. Preparation of copper nanoparticles by chemical reduction method using potassium borohydride. *Trans. Nonferrous Met. Soc. China* **2010**, *20*, s240–s244.
49. Cornell, R.M.; Schwertmann, U. *The Iron Oxides Structure, Properties, Reactions Occurrences and Uses*; Wiley-VCH: Weinheim, Germany, 1996.
50. Ismail, M.; Khan, M.I.; Khan, S.B.; Khan, M.A.; Akhtar, K.; Asiri, A.M. Green synthesis of plant supported Cu single bond Ag and Cu single bond Ni bimetallic nanoparticles in the reduction of nitrophenols and organic dyes for water treatment. *J. Mol. Liq.* **2018**, *260*, 78–91. [[CrossRef](#)]
51. Issaabadi, Z.; Nasrollahzadeh, M.; Sajadi, S.M. Green synthesis of the copper nanoparticles supported on bentonite and investigation of its catalytic activity. *J. Clean. Prod.* **2017**, *142*, 3584–3591. [[CrossRef](#)]
52. Karthik, K.V.; Raghu, A.V.; Reddy, K.R.; Ravishankar, R.; Sangeeta, M.; Nagaraj, P.S.; Reddy, C.V. Green synthesis of Cu-doped ZnO nanoparticles and its application for the photocatalytic degradation of hazardous organic pollutants. *Chemosphere* **2022**, *287*, 132081. [[CrossRef](#)]
53. Yadav, D.; Subodh, S.K. Awasthi, Recent advances in the design, synthesis and catalytic applications of triazine-based covalent organic polymers. *Mater. Chem. Front.* **2022**, *6*, 1574–1605. [[CrossRef](#)]
54. Arif Khan, M.; Nafarizal, N.S.; Mohd, K.A.; Chin, F.S. Surface Study of CuO Nanopetals by Advanced Nanocharacterization Techniques with Enhanced Optical and Catalytic Properties. *Nanomater* **2020**, *10*, 1298. [[CrossRef](#)]
55. Shinde, S.K.; Dubal, D.P.; Ghodake, G.S.; Fulari, V.J. Hierarchical 3D-flower-like CuO nanostructure on copper foil for supercapacitors. *RSC Adv.* **2014**, *5*, 4443–4447. [[CrossRef](#)]
56. Molazemhosseini, A.; Magagnin, L.; Vena, P.; Liu, C.C. Single-Use Nonenzymatic Glucose Biosensor Based on CuO Nanoparticles Ink Printed on Thin Film Gold Electrode by Micro-Plotter Technology. *J. Electroanal. Chem.* **2017**, *789*, 50–57. [[CrossRef](#)]
57. Vaseem, M.; Hong, A.R.; Kim, R.T.; Hahn, Y.B. Copper Oxide Quantum Dot Ink for Inkjet-Driven Digitally Controlled High Mobility Field Effect Transistors. *J. Mater. Chem. C* **2013**, *1*, 2112–2120. [[CrossRef](#)]
58. Manjari, G.; Saran, S.; Arun, T.; Vijaya Bhaskara Rao, A.; Suja, P.D. Catalytic and recyclability properties of phyto-genic copper oxide nanoparticles derived from *Aglaia elaeagnoides* flower extract. *J. Saudi. Chem. Soc.* **2017**, *21*, 610–618. [[CrossRef](#)]
59. Lakshmi, K.; Revathi, S. A facile route to synthesize CuO sphere-like nanostructures for supercapacitor electrode application. *J. Mater. Sci. Mater. Electron.* **2020**, *31*, 21528–21539.
60. Manoj, D.; Saravanan, R.; Santhanalakshmi, J.; Agarwal, S.; Gupta, V.K.; Boukherroub, R. Towards green synthesis of monodisperse Cu nanoparticles: An efficient and high sensitive electrochemical nitrite sensor. *Sens. Actuators B* **2018**, *266*, 873–882. [[CrossRef](#)]
61. Mugundan, A.; Rajamannan, B.; Viruthagiri, G.; Shanmugam, N.; Gobi, R.; Praveen, P. Synthesis and characterization of undoped and cobalt-doped TiO₂ nanoparticles via sol–gel technique. *Appl. Nanosci.* **2015**, *5*, 449–456. [[CrossRef](#)]
62. Govindaraj, R.; Pandian, S.M.; Ramasamy, P.; Mukhopadhyay, S. Sol–gel synthesized mesoporous anatase titanium dioxide nanoparticles for dye sensitized solar cell (DSSC) applications. *Bull. Mater. Sci.* **2015**, *38*, 291–296. [[CrossRef](#)]
63. Manikandan, B.; Rita, J. Impact of Ni metal ion concentration in TiO₂ nanoparticles for enhanced photovoltaic performance of dye sensitized solar cell. *Mater. Sci. Mater. Electron.* **2021**, *32*, 5295–5308.
64. Shamaila, S.; Sajjad, A.K.L.; Farooqi, S.A.; Jabeen, N.; Majeed, S.; Farooq, I. Advancements in nanoparticle fabrication by hazard free eco-friendly green routes. *Appl. Mater. Today* **2016**, *5*, 150–199. [[CrossRef](#)]
65. Foad, B.; Sajjad, S.; Mohammad, B.; Feisal, K. Biofabrication of highly pure copper oxide nanoparticles using wheat seed extract and their catalytic activity: A mechanistic approach. *Green Process. Synth.* **2019**, *8*, 691–702.

66. Sutradhar, P.; Debnath, N.; Saha, M. Microwave-assisted rapid synthesis of alumina nanoparticles using tea, coffee and triphala extracts. *Adv. Manuf.* **2013**, *1*, 357–361. [[CrossRef](#)]
67. Raveendran, P.; Fu, J.; Wallen, S.L. Completely “green” synthesis and stabilization of metal nanoparticles. *J. Am. Chem. Soc.* **2003**, *125*, 13940–13941. [[CrossRef](#)] [[PubMed](#)]
68. Koopi, H.; Buazar, F. A novel one-pot biosynthesis of pure alpha aluminum oxide nanoparticles using the macroalgae *Sargassum ilicifolium* A green marine approach. *Ceram. Int.* **2018**, *44*, 8940–8945. [[CrossRef](#)]
69. Sathya, S.; Murthy, P.S.; Devi, V.G.; Das, A.; Anandkumar, B.; Sathyaseelan, V.S.; Doble, M.; Venugopalan, V.P. Antibacterial and cytotoxic assessment of poly (methyl methacrylate) based hybrid nanocomposites. *Mater. Sci. Eng. C* **2019**, *100*, 886–896. [[CrossRef](#)]
70. Nabila, M.I.; Kannabiran, K. Biosynthesis, characterization and antibacterial activity of copper oxide nanoparticles (CuO NPs) from actinomycetes. *Biocatal. Agric. Biotechnol.* **2018**, *15*, 56–62. [[CrossRef](#)]
71. Rudramurthy, G.R.; Swamy, M.K.; Sinniah, U.R.; Ghasemzadeh, A. Nanoparticles: Alternatives against drug-resistant pathogenic microbes. *Molecules* **2016**, *21*, 836. [[CrossRef](#)]
72. Logpriya, S.; Bhuvaneshwari, V.; Vaidehi, D.; SenthilKumar, R.P.; Nithya Malar, R.S.; Pavithra Sheetal, B.; Amsaveni, R.; Kalaiselvi, M. Preparation and characterization of ascorbic acid-mediated chitosan–copper oxide nanocomposite for anti-microbial, sporicidal and biofilm-inhibitory activity. *J. Nanostruct. Chem.* **2018**, *8*, 301–309. [[CrossRef](#)]
73. Tulinska, J.; Mikusova, M.L.; Liskova, A.; Busova, M.; Masanova, V.; Uhnakova, I.; Rollerova, E.; Alacova, R.; Krivosikova, Z.; Wsolova, L.; et al. Copper Oxide Nanoparticles Stimulate the Immune Response and Decrease Antioxidant Defense in Mice After Six-Week Inhalation. *Front. Immunol.* **2022**, *13*, 874253. [[CrossRef](#)]
74. Grigore, M.E.; Biscu, E.R.; Holban, A.M.; Gestal, M.C.; Grumezescu, A.M. Methods of Synthesis, Properties and Biomedical Applications of CuO Nanoparticles. *Pharmaceuticals* **2016**, *9*, 75. [[CrossRef](#)]
75. Boliang, B.; Sivakumar, S.; Vaitheeswaran, D.; Muniasamy, S.; Naiyf, S.A.; Barathi, S.; Vinod, S.U.; Balasubramanian, M.G. Biosynthesized copper oxide nanoparticles (CuO NPs) enhances the anti-biofilm efficacy against *K. pneumoniae* and *S. aureus*. *J. King Saud Uni. Sci.* **2022**, *34*, 102120.

Disclaimer/Publisher’s Note: The statements, opinions and data contained in all publications are solely those of the individual author(s) and contributor(s) and not of MDPI and/or the editor(s). MDPI and/or the editor(s) disclaim responsibility for any injury to people or property resulting from any ideas, methods, instructions or products referred to in the content.